PHYSICAL REVIEW D VOLUME 47, NUMBER 11 1 JUNE 1993

ARTICLES

No 17 keV neutrino: Admixture < 0.073% (95% C.L.)

T. Ohshima, H. Sakamoto, T. Sato, J. Shirai, and T. Tsukamoto
KEK, National Laboratory for High Energy Physics, Tsukuba 305, Japan

Y. Sugaya and K. Takahashi
Tokyo University of Agriculture and Technology, Tokyo 184, Japan

T. Suzuki
RIKEN, Institute of Physical and Chemical Research, Wako 351-01, Japan

C. Rosenfeld and S. Wilson
University of South Carolina, Columbia, South Carolina 29208

K. Ueno
University of Rochester, Rochester, New York 14627

Y. Yonezawa*
Institute of Applied Physics, University of Tsukuba, Tsukuba 305, Japan

H. Kawakami, S. Kato, S. Shibata, and K. Ukai
Institute for Nuclear Study, The University of Tokyo, Tokyo 188, Japan
(Received 12 January 1993)

To solve the controversial issue concerning the possible existence of a 17 keV neutrino with a 1% admixture in nuclear β decay, we searched directly for any evidence of a production-threshold effect. The ^{63}Ni β spectrum was measured with a magnetic spectrometer, with very high statistics along with a fine energy scan over a narrow energy region around the expected threshold. The obtained mixing strength was $|U|^2 = [-0.011 \pm 0.033(\text{stat}) \pm 0.030(\text{syst})]\%$, very consistent with zero, and decisively excluding the existence of a 17 keV neutrino admixing at the 1% level with the electron neutrino. The corresponding upper limit was set at $|U|^2 < 0.073\%$ (95% C.L.). A new limit was also obtained for a wider mass range: $|U|^2 < 0.15\%$ (95% C.L.) for 10.5 to 25.0 keV neutrinos.

PACS number(s): 23.40.Bw, 14.60.Gh, 27.50.+e

I. INTRODUCTION

Extensive experimental efforts continue in order to probe the basic properties of the mysterious neutrinos. The current issues are related to their masses and flavor mixing. In addition to the solar neutrino problem, in particular, an experimental indication of a 17 keV neutrino, reported by Simpson [1] in 1985, has added fuel to neutrino studies. Various theoretical models [2] have been proposed to accommodate such particles, while experimental investigations have become controversial.

The current experimental situation regarding the 17 keV neutrino is illustrated in Fig. 1. There is a clear discrepancy between the negative [3–12] and positive [13–17] results, which cannot be due to statistical fluctuations. One might say that since positive evidence has been obtained only in experiments using solid-state detectors, not using magnetic spectrometers, unknown detector-related phenomena are yielding an effect which resembles a heavy-neutrino contribution. If so, the unknown phenomena have something to do with the specific energy (17 keV) below the end-point energy since the possible mass values so far reported are all around 17 keV [18], irrespective of the kind of nuclei used for experiment. On the other hand, measurements using a magnetic spectrometer have been criticized as having some ambiguities regarding the β-ray spectral correction.

The search for a heavy neutrino involves looking for some distortion due to neutrino mixing in the β-ray spectrum or an internal bremsstrahlung γ-ray spectrum associated with some electron-capture process of radioactive nuclear decays. The flavor eigenstate could be a linear

*Present address: Tsukuba College of Technology, Tsukuba 305, Japan.

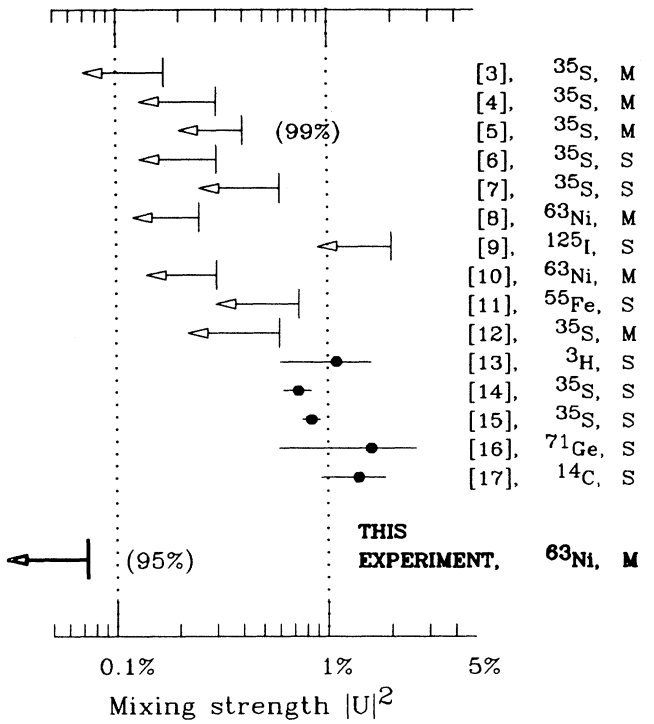

FIG. 1. Experimental results concerning the mixing strength ($|U|^2$) for 17 keV neutrino. The arrows represent the upper limits at the 90% confidence level (unless otherwise indicated), while the closed circles are from experiments reporting positive evidence. Indicated on the right are the reference, the β-ray emitter, and the experimental method. M and S represent a magnetic spectrometer and a solid-state detector, respectively. Our result is also indicated by the thick arrow.

combination of the mass eigenstates: $|\nu_e\rangle = \cos\theta\,|\nu_1\rangle + \sin\theta\,|\nu_2\rangle$ if only two states are considered, where θ represents the mixing angle. The β spectrum would thus be

$$N(E) = \cos^2\theta N_1(E) + \sin^2\theta N_2(E), \quad (1)$$

$$N_i(E) = F(Z,E)pE_T(E_0-E)\sqrt{(E_0-E)^2-m_i^2}$$

$$(E < E_0 - m_i;\ i = 1,2),$$

where p, E, and E_T are the momentum, kinetic energy, and total energy of a β ray. E_0 is the end-point energy and $F(Z,E)$ is the Fermi function. For the case in question, the mass m_1 of the dominant neutrino, $|\nu_1\rangle \simeq |\nu_e\rangle$, is set to zero and mass m_2 to 17 keV. Thus, the minor $|\nu_2\rangle$ component should manifest itself as an excess over the major term at an energy below its emission threshold, $E_{\rm th} = E_0 - m_2$. Such an excess corresponding to $\sin^2\theta \sim 1\%$ was reported as positive evidence for a 17 keV neutrino [1,13–17]. (In the following, the admixture $\sin^2\theta$ is denoted by $|U|^2$.) For the sake of intuitive understanding, the spectrum is usually presented in the form of a Kurie plot: $\sqrt{N(E)/[F(Z,E)pE_T]}$ vs E. It forms a straight line if $|U|^2=0$; for $|U|^2\neq 0$, however, the slope for $E \ll E_{\rm th}$ is different from that for $E \geq E_{\rm th}$. Although the experimental principle is very simple, getting a reliable measurement is not, as described below.

History is our teacher: for instance, it had already been found 58 years ago in 1934 [19], a few years after the birth of Fermi's β-decay theory, that Kurie plots of the measured β-ray spectra were not as straight as theoretically expected. A noticeable excess was seen in the low-energy part of the spectrum. This discrepancy was at that time interpreted as being an indication of the necessity to revise Fermi's theory, not as a sign of heavy-neutrino production. For example, Konopinski and Uhlenbeck [20] even proposed a revised theory in 1935 in order to explain the experiment. Various investigations [21], which were carried out for over 20 years, finally revealed that the low-energy excess was the result of energy losses in the source substance and backscattering at the source backing plate. It is interesting to realize that we are again facing controversy concerning the β-ray spectral shape. This time, however, it is frequently interpreted as arising from a 1% admixture of a 17 keV neutrino, thus causing some excitement among particle physicists.

We performed a measurement in order to clearly solve this controversial situation concerning the proposed 17 keV neutrino with a 1% admixture. It was aimed at achieving a sensitivity of 0.1% on $|U|^2$ by directly searching for a kink of the expected emission threshold in the ^{63}Ni β spectrum with high statistics and under well-controlled systematic conditions. Our experimental strategy to overcome the problematic aspects of previous experiments is described in Sec. II. Descriptions of the experimental apparatus and the quality examination of the observed data are given in Secs. III and IV, respectively. Section V presents deductions concerning the β spectra and the response function. An analysis of the β spectra in terms of a χ^2 fit is performed in Sec. VI, but using a somewhat different method than that used in a previous publication [22]. Two analyses resulted in very good agreement concerning every fitting variable in detail. A further examination of the observed β spectra is presented in Sec. VII. The search for a different mass of the heavy neutrino is also described in Sec. VI.

II. CONSIDERATION

A. Objectives

1. *Low-energy tail of R(E) and the shape correction*

The true β spectrum is deformed due to the finite resolution of the experiment. This effect is represented by the response function $R(E',E)$, which gives the probability for monoenergetic electrons of energy E' to be detected at energy E. [For simplicity, $R(E',E)$ is hereafter denoted as $R(E)$ throughout most part of this paper.] A long, low-energy tail appears in $R(E)$ due to energy losses and backscattering, which exhibits an approximately flat

energy distribution with an amplitude of δ (keV)$^{-1}$ down to zero energy. We also describe the fact that a fraction of the β rays of energy (E') flows into a data point at a lower energy E. By approximating the true spectrum $N(E)$ to be proportional to the square of the energy interval from the end point, E_0, the fractional size of the tail contribution to the observed spectrum can be estimated as

$$\frac{\text{tail effect}}{N(E)} \sim \frac{\int_E^{E_0} \delta N(E')dE'}{N(E)} \sim \frac{\delta}{3}\Delta E, \qquad (2)$$

where $\Delta E \equiv (E_0 - E)$. In an experiment with a β source separated from a detector, the backscattering generates a tail with a size of 20–30 % of $R(E)$. δ is thus on the order of 10^{-3} (keV)$^{-1}$. For example, δ ~(20–30 %)/(~150 keV) for an ^{35}S source (E_0=167 keV). Then, the above-mentioned cumulative effect easily results in an excess of a few %, since the net effect is amplified by a factor of ΔE, which is typically a few tens of keV.

Such an excess at lower energies never disappears, even though it can be reduced by experimental efforts. Systematic uncertainties usually limit any knowledge concerning δ to $\sim 10^{-4}$ (keV)$^{-1}$, thus leaving some 10^{-3} ambiguity in the measured spectrum, which cannot be ignored in a search for a heavy-neutrino effect at the 1% level. A so-called shape correction term is thus introduced to absorb this ambiguity. The term should never be omitted, unless experimentally justified.

2. Statistical balance and wide energy spectrum

Most of the previous experiments measured some spectrum over a wide energy region, and used a χ^2 fit over all parts in order to look for any difference in the slopes above and well below $E_{\rm th}$, the threshold energy for heavy-neutrino emission. Nobody, except for Hetherington *et al.* [10], obtained sufficiently high statistics in the higher side to determine the slope there. In such data, the lower is the β-ray energy, the higher is statistical accuracy, though the ambiguity is larger due to the tail effect described above. The situation is reversed at higher energies. Consequently, the analysis becomes strongly biased by the low-energy portion of the data where the uncertainty is large.

The above problem is not easily solved in experiments using a solid-state detector. The usable source intensity is severely limited by a signal pileup effect. Further, no β rays in an energy band of interest can be singled out.

3. Signal-to-background ratio

Accurate knowledge concerning background is, needless to say, the key for any reliable result. The determination of the slope above $E_{\rm th}$ is particularly affected by the background. Experiments using solid-state detectors suffer from a signal pileup effect and residual radioactivity. In fact, the signal-to-background ratio was only 6–60 near $E_{\rm th}$ in such experiments [13–17]. A magnetic spectrometer can considerably improve this situation.

B. Experimental strategy

Along with these considerations, we adopted a strategy to search directly for a kink due to the proposed 17 keV neutrino emission by means of a fine scan over the narrow energy region in question with equally high statistics both above and below $E_{\rm th}$. Any systematic uncertainties possibly arising from the energy-dependent character of corrections would not be a significant factor in a kink search. A kink, if it exists, would not be confused with the shape correction term. A very high-statistics measurement was made possible due to the combination of an intense source (^{63}Ni) and a high-resolution magnetic spectrometer. The signal-to-background ratio was as high as 1000 near $E_{\rm th}$, thus reducing the ambiguities in the background estimation to an insignificant level.

Another important feature of the present experiment is that $R(E)$ was precisely determined by a measurement, not by a Monte Carlo simulation. A monoenergetic β emitter (^{109}Cd) was used for this purpose, which was prepared so as to yield the same energy-loss and backscattering effects as that of the ^{63}Ni source.

The spectrum near E_0 was also measured at a place where the shape correction is negligible and the 17 keV neutrino has no effect. The thus-obtained E_0 value was compared, as a self-consistency test, with those determined by data taken around $E_{\rm th}$. The measurement was carried out using 30 independent cells of a proportional chamber; this also helped in examining any systematic effects.

III. APPARATUS

A. β spectrometer

The β-ray momentum was analyzed by a double focusing $\pi\sqrt{2}$-type, iron-free spectrometer at INS (Institute for Nuclear Study). This spectrometer had been successfully used in previous experiments [23] with a thin tritium source in order to set the limit on the mass of the electron antineutrino. The mean radius of the β-ray orbit is 75 cm, the main coil current is stabilized to within 10^{-5}, and three sets of Helmholtz coils (east-west, north-south, and up-down) can cancel an external magnetic field and its fluctuation down to 10^{-6} of the 10 G field applied to the β rays. The momentum resolution is controlled by a discrimination baffle slit located at 60° from the source position (see Fig. 2). For this experiment, the slit was adjusted so as to give $\Delta p/p$=0.2% and a solid angle of $\Omega/4\pi$=4.7×10^{-3}. The vacuum of the spectrometer chamber was kept at 10^{-3}–10^{-4} Pa during the entire period.

B. β source

We employed ^{63}Ni ($\tau_{1/2}$=100 yr) and ^{109}Cd ($\tau_{1/2}$=463 days) radioactive nuclei as the experimental and calibra-

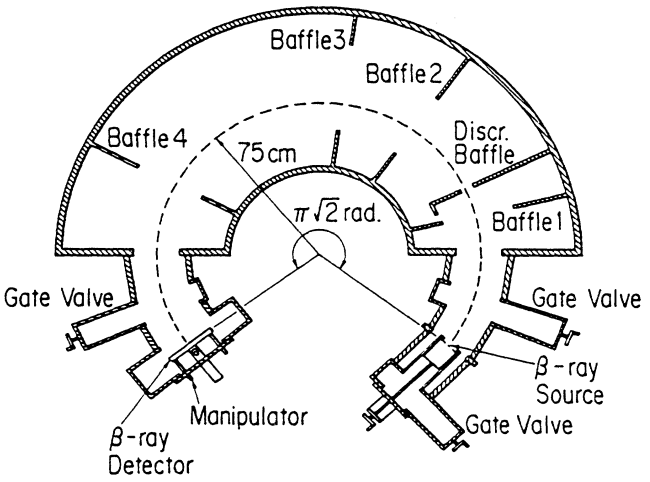

FIG. 2. Top view of a vacuum chamber of the INS $\pi\sqrt{2}$-type, iron-free spectrometer. The momentum resolution is controlled by a discrimination baffle slit.

tion β emitters, respectively. ^{63}Ni provides a 12-times larger rate decaying into energies near $E_{\rm th}$ than does ^{35}S. Well-known conversion lines of ^{109}Cd decay provide us with a means to calibrate the system as well as to determine $R(E)$. The two sources were alternated several times during the experiment. The reproducibility of the source position was verified using the measured relative shift of the K conversion lines between different calibration runs, to be better than $\leq \pm 60$ μm, equivalent to $\Delta E \leq \pm 2$ eV at E=50 keV. The sources were electrically grounded in order to avoid any charging.

Both sources, each of 4×20 mm^2 size, were prepared on a 1.5 μm thick Ni backing foil by an electroplating method under the same conditions. An electrolytic solution (0.5 ml) of 1% ammonium lactate was used for the electroplating process with a constant 10 V applied for 15 min at room temperature. The electric current in this process ranged from 40 to 80 mA. The thus-obtained ^{63}Ni source was 50 μg/cm^2 in thickness and 580 μCi in intensity.

The ^{109}Cd source of 150 μCi was prepared as a mixture with natural Ni atoms so that the energy-loss and backscattering effects would be the same as those produced with the ^{63}Ni source. The uniformity of the mixture was confirmed in two ways. (1) The electroplated efficiency was measured as a function of time by counting the β intensity. The same efficiency was observed for two solutions (^{63}Ni mixed with natural Cd and ^{109}Cd mixed with natural Ni). (2) Another source was made by electroplating the correct amount of ^{109}Cd and then natural Ni. The amount of the latter was just one-half that contained in the standard ^{109}Cd source. Since natural Ni dominates the material in the standard ^{109}Cd source, this choice was made in order to mimic the average energy losses encountered in the standard one. In fact, the same K line shape was observed for the standard and this test source. Finally, six ^{109}Cd sources were prepared, and measurements were made for each of them concerning the line shape and the count rate. The result verified good reproducibility in the source preparation.

C. β detector

The β detector was a proportional wire chamber with 30 isolated cells placed on the spectrometer focal plane. Fig. 3 shows its structure. Signal wires were of 20 μm ϕ Au-plated tungsten, strung at 6 mm intervals. Rectangular counting cells of 5×6 mm^2 each were formed by inserting 1 mm thick brass walls. Facing the incident β rays, an entrance slit of 3×40 mm^2 opening was cut out for each cell on a 1 mm thick brass plate. The slit size corresponds to the momentum bite of $\Delta p/p$=0.1% or an energy bite of ΔE=96 eV at E=50 keV. Behind the slit plate was a 1.5 μm polyester film sandwiched by 100 μm thick stainless-steel meshes of 95% in transparency. It isolated the chamber gas from the spectrometer vacuum and the inner mesh served as a cathode plane. The counting gas was isobutane kept at 4×10^4 Pa (within 1%). A high voltage of 1.54 kV was applied in order to keep the counting loss sufficiently small. Preamplifiers

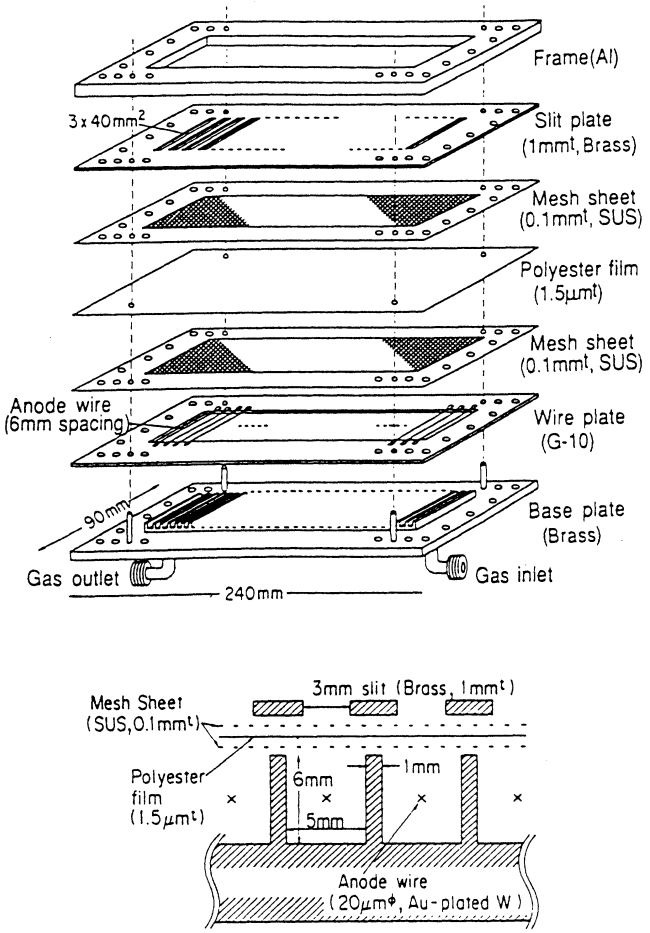

FIG. 3. Structure and construction of the proportional chamber used as the β-ray detector.

were mounted on the chamber. The position and angle of the source and detector were optimized for the best momentum resolution by observing the ^{109}Cd K line. In this paper, the cells are numbered 1–30 from the low- to high-momentum side.

D. Data acquisition system

The electronics system is illustrated in Fig. 4. The overall gain in each pre- and post-amplifier chain was 12 mV/μA. Amplified signals were sent to analogue-to-digital converters (ADC's) (LeCroy FERA) for pulse-height measurements as well as to discriminators. The discriminator outputs were useful in three ways: to record the numbers of hits/cell by scalers, to register any event hit pattern by the ADC's, and to tag the hit multiplicity by the multiplicity logic module (LeCroy 380A). Multiple hits were caused by cosmic rays, electronic noise, and cross talk; their rate was used to correct for the dead time. Since electronic noise manifested itself as simultaneous trailing pulses on many cells, a 500 μs wide inhibit signal was generated on the multiplicity $N \geq 3$. Its contribution to the dead time, however, was negligibly small.

The magnetic field strength of the spectrometer was set by a standard voltage generator (FLUKE 5440A). Using two digital multimeters (FLUKE 8505A's), a μVax computer was used to monitor the generator voltage as well as the voltage across a standard resistor inserted in series with the main coil, and thus controlled the generator accordingly.

IV. DATA-TAKING AND QUALITY EXAMINATION

A. Data-taking procedure

The ^{63}Ni spectrum was measured in two different energy regions: One was around the expected heavy-neutrino emission threshold (called the $E_{\rm th}$ region) and the other was around the end point (the E_0 region). As illustrated in Fig. 5, three sets of scans covered the energy regions of interest. Each set consisted of measurements performed at 20 magnetic fields approximately in 284 eV steps for the $E_{\rm th}$ region and the 4 magnetic fields approximately in 7.4 keV steps for the E_0 region. In the former, the number of data points totaled (3 sets)$\times$ (20 magnetic fields per set)$\times$(30 detector cells)=1800. Of the 20 points in each scan set, as can be seen in the figure, 3 points always overlapped with one or two other sets for normalization purpose.

At each magnetic field setting (thereafter expressed by the voltage across the standard resistor, $V_{\rm mag}$), a measurement lasted 5 min, generating 30 data points corresponding to the number of detector cells. In order to minimize any systematic errors, the $V_{\rm mag}$ value at every scan was selected randomly. This was repeated until more than 10^6 counts had been accumulated at every data point, resulting in 2.4×10^9 total events over the $E_{\rm th}$ region where the signal-to-background ratio was as high as 1000. Typical counting rates were 40 Hz and 0.03 Hz/cell at $E_{\rm th}$ and above E_0, respectively.

The ^{109}Cd spectrum measurement was performed over a wide energy region from 16 to 107 keV in order to cover the KLL Auger, K, L, M and N conversion lines. Different scanning steps were chosen, depending on the purpose: an absolute energy calibration, a measurement of the spectrometer dispersion (dp/dx, where x is position displacement on the detector plane), or a measurement of the response function. Figure 6 shows an example of such data recorded on the 16th cell. The counting rate was

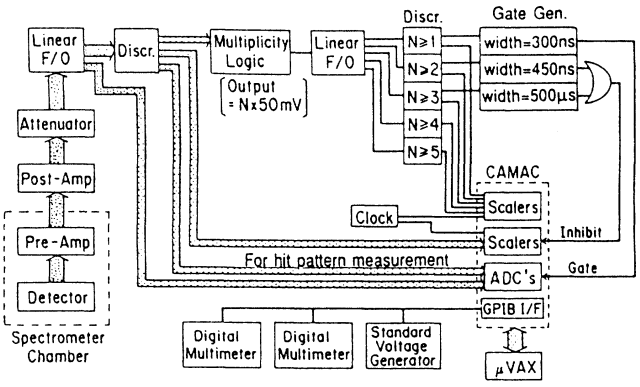

FIG. 4. Electronics diagram.

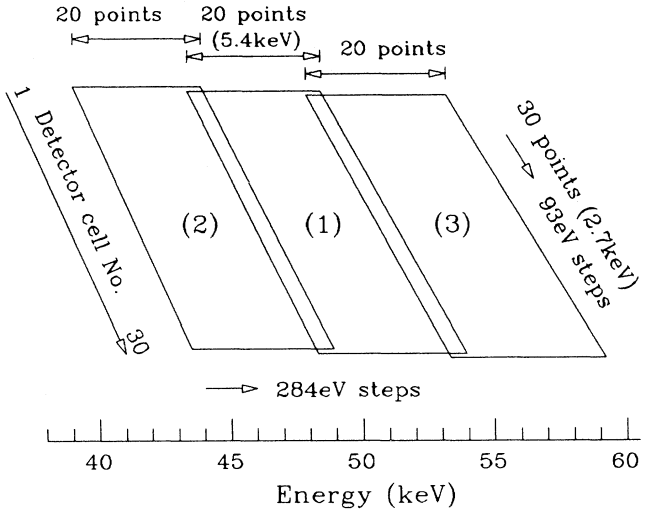

FIG. 5. Illustration of an energy scan performed around the 17 keV neutrino threshold, $E_{\rm th}$=50 keV. Each of the three sets of scans covered a diamond-shaped area, comprising (20 $V_{\rm mag}$ settings)$\times$(30 detector cells)=600 data points. The overlapped zones comprised three data points per detector cell from each neighbor. The energy regions covered by the 16th cell are 45.9–51.3 keV in (1), 41.4–46.5 keV in (2), and 50.7–56.3 in (3). The four points in the E_0 region, not illustrated, covered 65.4–87.6 keV in (1), 68.9–91.5 keV in (2), and 63.7–85.7 keV in (3).

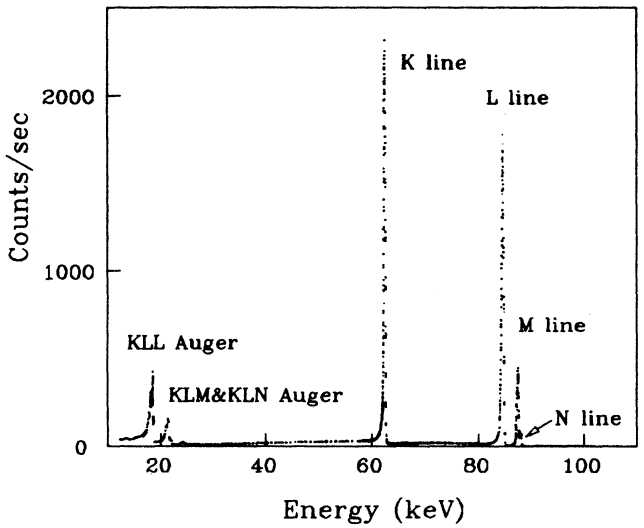

FIG. 6. ^{109}Cd spectrum measured in the 16th detector cell, showing discrete lines and their tails used for calibration purposes.

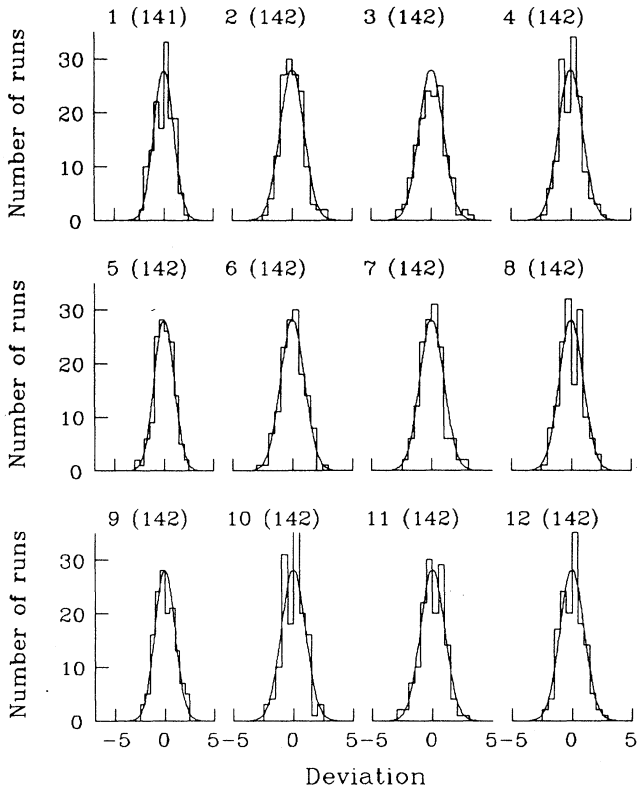

FIG. 7. Distributions of the counting rates (n's) relative to the average ($\bar{n}$). The horizontal axis corresponds to $(n\text{-}\bar{n})/\sqrt{\bar{n}}$. The data are from the 16th detector cell, in data set (1) at 12 different $V_{\rm mag}$ settings. The curves are Gaussians of unit standard deviation, with areas equal to the number of runs shown in parentheses.

2.2 kHz/cell at the peak of the K line. The measurement was performed four times during a 2-month data-taking period, each lasting for 2 to 3 days.

The background was studied without the source, or by closing gate valves at either the source chamber or the detector chamber. Since it was mostly cosmic rays, the rate did not appreciably depend on how the β rays were shut out. In addition, this rate fairly well agreed with those observed above E_0 (>67 keV) as well as above the Cd N line (>88 keV) where no β rays should exist.

B. Data quality

1. ^{63}Ni data

As explained above, each data point is a result of many runs performed in random order. The run-to-run stability of the counting rates in individual detector cells should be a good measure of the data quality. The histograms in Fig. 7 show distributions of the rates (n's) recorded under identical conditions. The curves are Gaussian distributions normalized to the respective number of runs. One clearly finds only statistical fluctuations without any extra disturbance. This is also true for all of the other data not shown in the figure. The counting rates of all runs at 600 individual data points, (20 $V_{\rm mag}$'s)×(30 cells), in the $E_{\rm th}$ region were further examined in terms of the reduced χ^2:

$$(\text{reduced } \chi^2) \equiv \sum_{\text{run}} \left(\frac{n - \langle n \rangle}{\sqrt{n}} \right)^2 \Big/ [(\text{the number of runs}) - 1]. \tag{3}$$

Here, $\langle n \rangle$ corresponds to the average of the rates at each data point, and is determined by minimizing the reduced χ^2. Figure 8 shows the reduced χ^2 distributions for the three sets of scans. The curves represent ideal χ^2 distributions and show that the data scatter in a purely statistical manner.

As shown in Fig. 5, three sets (1, 2 and 3) of scans were carried out in random order for individual points, with an overlap in two bands. The ratio of the summed counts in these bands should depend only on the data-collection time and the ^{63}Ni lifetime. The experimental values are 0.424 30±0.000 06 for (2)/(1) and 1.328 09±0.000 18 for (3)/(1), which are in very good agreement with the expected 0.424 45 and 1.3299.[1]

[1]Because there was a scheduled electric power outage after scans (1)–(2), the comparison of the absolute rates between (1) and (3) gets a bit poor. But, it does not influence this experiment. The ^{109}Cd calibration runs were therefore performed before and after the both (1)–(2) and (3) scans

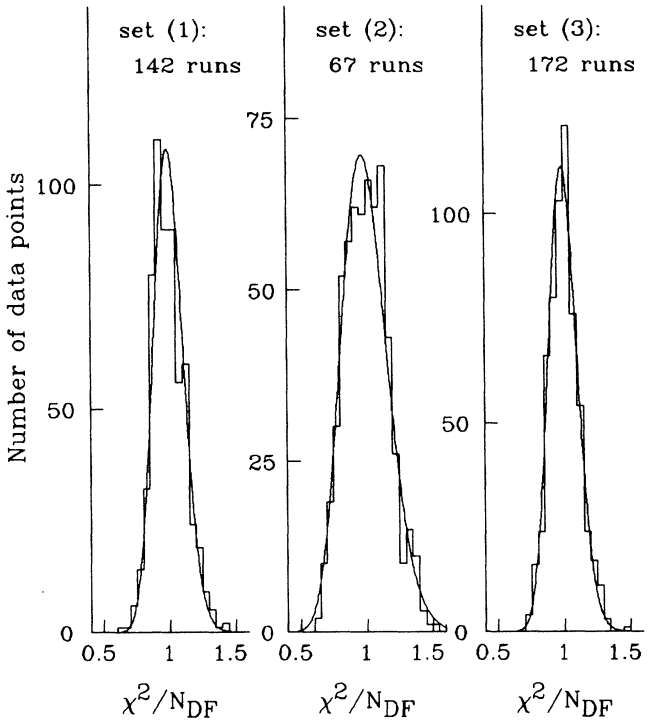

FIG. 8. Histograms of reduced χ^2 defined by Eq. (3) for three data sets, each with 600 data points. The curves represent ideal distributions for Gaussian distributed variables for the corresponding number of runs.

It is thus concluded that the entire experimental system has been stable and that the final spectrum can be obtained by summing all of the counts in each detector cell at the same V_{mag} without making any time-dependent corrections. A single scan set lasted for about 2 h at over 24 different V_{mag} settings with 5 min each. The long life of ^{63}Ni does not require any correction for this time period, and the random sequence in the individual settings further reduced the effect of the source lifetime. It can also be concluded that the source did not evaporate in a vacuum, contrary to other cases [8,12].

2. ^{109}Cd data

Of the four calibration data sets with the ^{109}Cd source, both the first two and second two were taken at 29–30 day intervals. The source lifetime is not negligible here when comparing the data sets. The observed ratio of counts at around the K line is 0.9568 between the first two and 0.9569 between the second two, while 0.9561–0.9575 is expected for both from the decay in the source intensity. This agreement again confirms the stability of the system, as already shown using the ^{63}Ni data. It also shows that no appreciable source evaporation occurred.

V. DATA REDUCTION

We aimed at precisely measuring the shape of the ^{63}Ni β-ray spectrum, not the absolute decay rate. Therefore, energy-dependent corrections were important, such as the electronics dead time, transmission through the detector window, and any loss due to pulse-height discrimination. The Cd spectrum was used for absolute-energy calibration as well as to establish the spectrometer dispersion. The response function [$R(E)$] was also obtained from the same data. Finally, the Ni β-ray spectra in 30 individual cells were arranged for subsequent analyses.

A. Corrections

1. Dead time correction

The scaler counts of 30 cells at every V_{mag} setting were normalized by the live-time interval. Only single-hit events were counted in order to reject electronic noise, cosmic rays, and cross talk. The number of inhibit signals generated on multihit events was also recorded in order to evaluate the electronic dead time. The resulting dead time correction was on the order of 10^{-4} for 20 points in individual data sets, each covering approximately a 5.4 keV interval near E_{th}. Its variation between the lowest- and highest-energy point was 3×10^{-4} for set (1), 4×10^{-4} for (2), and 2×10^{-4} for (3). Consequently, this correction of the ^{63}Ni spectral shape amounted to only $\leq \pm2\times10^{-4}$ over the 5.4 keV interval near E_{th}. The correction near E_0 was even smaller, being on the order of 10^{-5}.

2. Count loss due to discrimination

The background pulse-height distribution in the chamber was determined from data taken at two V_{mag} settings, where no β rays from the source were expected. Figure 9(a) shows a typical background-subtracted pulse-height distribution for the Ni source. One can see a discrimination level corresponding to ADC channels of 10 or below; the loss due to discrimination is therefore only a small fraction of the total events. What is relevant in this experiment is the β-ray energy dependence of this small fraction.

The low pulse-height part is shown in Fig.9(b), where 20 spectra corresponding to 20 consecutive V_{mag} settings in one of three data sets are plotted for the same detector cell, and the histogram is their average. The fraction of counts in this part does not show any noticeable dependence on the β-ray energy (or V_{mag}). To determine the possible energy dependence of some discrimination effect, the count integrated over low ADC bins was studied relative to the average, by defining

$$\epsilon(E) \equiv \int_0^{c_{max}} h(E,c)dc \Big/ \int_0^{c_{max}} \overline{h}(E,c)dc, \qquad (4)$$

where $h(E,c)$ represents the count in the cth ADC bin for the β-ray energy (E) and $\overline{h}$ is the average of 20 spectra. $\epsilon(E)$ depended slightly on the range of integration. The choice of c_{max}=9 was made in order to make it sensitive to any discrimination effect. The result is plotted in

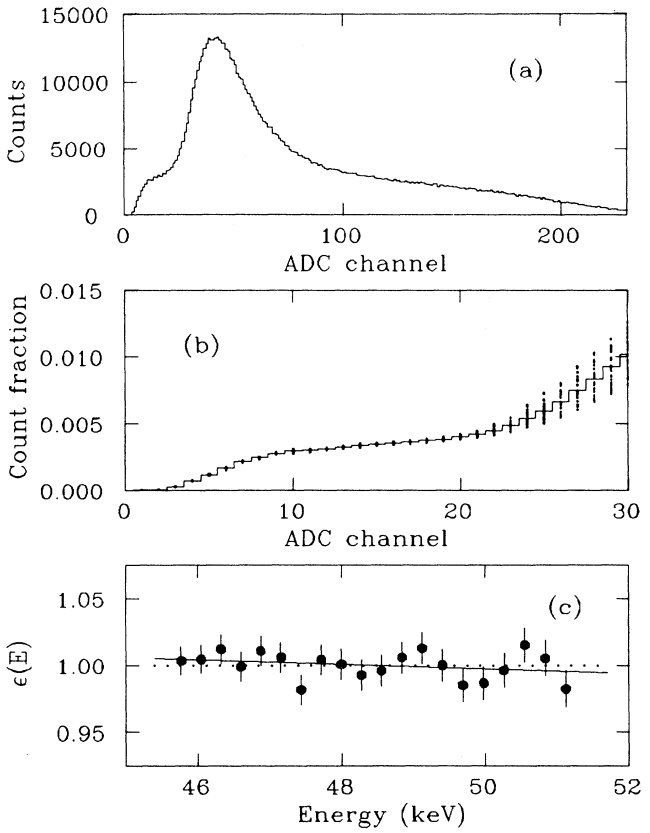

FIG. 9. (a) Background-subtracted pulse-height distribution for the 15th detector cell measured at the 10th $V_{\rm mag}$ setting in data set (1). (b) A closeup of the low pulse-height region of (a). The dots are for 20 different $V_{\rm mag}$ settings and the histogram shows their average. (c) $\epsilon(E)$ defined by Eq. (4) at individual $V_{\rm mag}$ values, thus at different E. The solid line is a fit to the data.

Fig.9(c) as a function of E. The linear fit shown in the same figure gives the energy-dependent contribution to the low pulse-height part to be smaller than ±1%/keV. The total loss of counts in this pulse-height region was (1.5±0.4)%, by linearly extrapolating the counts at $c_{\rm max}$. The uncertainty resulted from the fact that the choice of $c_{\rm max}$ is not unique. The final correction factor is therefore less than $(1.5\pm0.4)\times10^{-4}$/keV. The same correction was also applied to the Cd spectrum, although it is much smaller than the statistical errors.

3. Transmission of detector window film

The only material to be considered is the 1.5 μm thick polyester used as the detector window, since the meshes have a fixed transmission, irrespective of the β-ray energy of interest. The chemical structure of the film is $C_{2+10n}H_{6+8n}O_{2+4n}$ and the density is 1.393 g/cm^3. For sufficiently large values of n, the effective atomic and mass numbers are $Z_{\rm eff}$=6.45 and $A_{\rm eff}$=12.39, respectively. The ambiguities in the n value has totally negligible effects on the transmission.

Semiempirical equations exist that relate the electron energy and the extrapolated range [24], and that represent the transmission [25]. Equations (6) and (7) in Ref. [24] well reproduce many experimental data; however, as the authors pointed out, they are not in perfect agreement with each other. This uncertainty corresponds to approximately ±4% in our film thickness, while the actual thickness is uncertain to ±3%. Thus, by quadratically adding these uncertainties, ±5% was assigned as a systematic error in the film thickness.

Figure 10 shows the thus-calculated transmission through the 1.5 μm film, which is 98.1% at E=40 keV to 99.3% at E=60 keV. The range of uncertainty is also shown there, and is smaller than $\pm1\times10^{-3}$ in the $E_{\rm th}$-region. This correction was also applied to the Cd spectrum.

B. Energy determination

1. Dispersion relation

The momentum dispersion of the spectrometer was established by determining the $V_{\rm mag}$ value, $V_{K\ \rm line}$, at which the Cd K line peak appeared in a given detector cell. For this purpose, by changing $V_{\rm mag}$, the position of the K line was moved across all of the cells. The accuracy in this measurement was ±(1–2) eV in energy. The result was fit by a fourth-order polynomial of the cell number (j), where the 16th cell was taken as a reference:

$$(V_{K\ \rm line})_j(V) = (V_{K\ \rm line})_{16}(V)[1 + a(j-16) + b(j-16)^2 + c(j-16)^4]. \quad (5)$$

The sizes of the coefficients determined in the first cal-

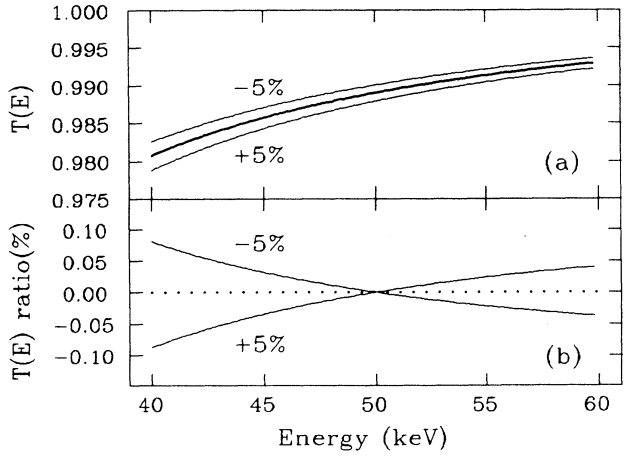

FIG. 10. (a) Calculated β-ray transmission [$T(E)$] for a 1.5 μm thick polyester film. The thin curves show the range of uncertainty corresponding to ±5% of the nominal thickness. (b) The range of relative uncertainty when normalized at E=50 keV.

ibration run came out to be $a = -1.950\,23\times10^{-3}$, $b = 6.345\,26\times10^{-6}$, and $c = 3.071\,30\times10^{-9}$. They agreed very well with the analytic orbital calculation.

The same measurement was performed in every calibration run. A slight variation which depended on the run was detected in the $V_{\rm mag}$ value for the K peak at the reference cell, and was attributed to a source replacement error. By examining the relative shift of the K and L lines, the errors in position were found to be ±15 μm between the first two calibrations and ±60 μm between the second two. They correspond to an energy uncertainty of ±0.6 eV and ±2.4 eV at K line energy.

2. *Absolute-energy calibration*

To relate $V_{\rm mag}$ to the β-ray momentum, the K and L lines, as well as the KLL lines, were measured by the 16th cell in every calibration. Their energies (and relative intensities) are known with accuracies of 0.3–0.4 eV for the K and L lines [26] as well as 1.3–1.7 eV for the KLL lines [27]. In our measurement, the K line, E_K=62.520 keV, was measured with an accuracy of $\pm0.7\times10^{-5}$ in $V_{\rm mag}$, or ±0.8 eV in energy. A fit was made to the L line data based on the observed K line spectrum, rescaled by taking into account the energy differences, the relative intensities of the L sublines, and the different energy losses. The result was accurate to $\pm3.1\times10^{-5}$ in $V_{\rm mag}$, or ±4.9 eV in energy, at E_{L_3}=84.683 keV. The KLL Auger spectra were fit by a functional form used in Ref. [27]; the KL_2L_3 line, $E_{KL_2L_3}$=18.512 keV, was determined to be $\pm6.8\times10^{-5}$ in $V_{\rm mag}$ or ±2.5 eV in energy.

The result is expressed as

$$p(\mathrm{keV}/c) = 187.6650 \times V_{\rm mag}(\mathrm{V}) + 0.3070 \qquad (6)$$

for the 16th cell. This relation was valid for all of the calibration runs within ±1 eV accuracy and, therefore, at all of the energies covered by Ni runs.

Equations (5) and (6) were used to convert the $V_{\rm mag}$ value of each data point to the energy E. The measured counts at all of the points were then corrected so as to have the same energy bin size.

C. Response function

Because of the optical characteristics of the spectrometer, there is a very small cell dependence in K line spectra. The momentum resolution [$\Delta p/p$ full width at half maximum (FWHM)] varies parabolically from 0.26% at the 16th cell to 0.29% at both ends (1st and 30th cells). In more detail, their half width at half maximum (HWHM) remains constant at the higher-momentum side, but has a cell dependence at the lower side. Therefore, both Ni and Cd spectra measured in individual cells were separately treated in the following analyses.

To extract only the K line spectrum from the data (shown in Fig. 6, for example), the low-energy tails of the L and higher lines must be subtracted. They were assumed to have the same functional forms as that of the K line. In the spectrum, small but broad bumps were observed near 53 and 72 keV, which could be backscattered β rays of the K and L lines, respectively. Because of this effect, the tail shape, expressed as $\exp[(E_{\rm bump} - E)^{1.5}]$, where $E_{\rm bump}$ represents the position of the bump, was found to reproduce the data. Several different functions were also used to evaluate the uncertainty in the subtraction. Figure 11 is a result of such an evaluation, showing the possible variations in the tail spectrum. This uncertainty was treated as one of the systematic errors in the final analyses to be described later. The high-energy side of the resulting pure K line shape was also checked by comparing it with that of the N line, which is at the highest energy receiving no contribution from other conversion lines.

Figure 11 shows the thus-obtained K line spectrum. It is equivalent to the response function $R(E_K, E)$ for β rays of energy E_K. The low-energy component reflects the backscattering and energy-loss effects. This response function was applied to other β-ray energies by just rescaling it in momentum.

D. ^{63}Ni spectrum

After applying the conversions and corrections described above, the counts recorded under the same conditions were summed. As described before, there were 1800 data points near $E_{\rm th}$, and 360 data points at around E_0. The three sets of data were normalized using the counts in the overlapped region, three points from each set. The

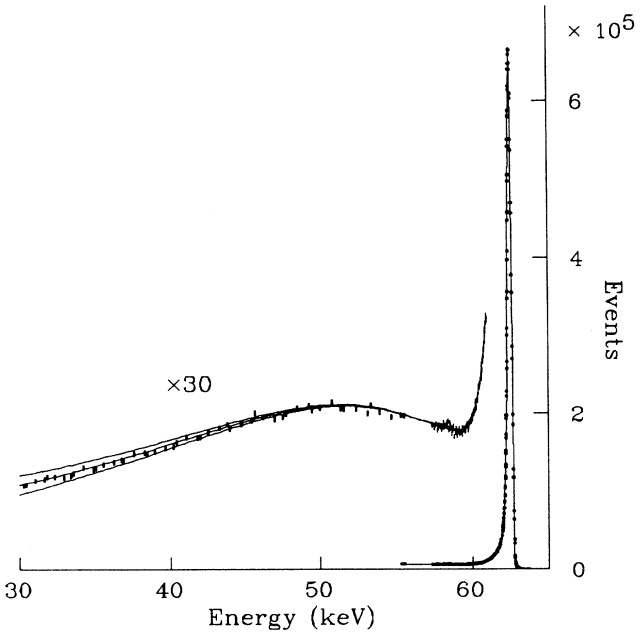

FIG. 11. Response function [$R(E_K, E)$] extracted from the ^{109}Cd β spectrum, shown by a curve with data points. The size of the ambiguity resulting from subtraction of the L and higher line components is indicated, by adding to the $R(E_K, E)$, by upper and lower curves.

normalization factors for each cell are

$$\xi_1 = \sum_{k=18}^{20} n_1(k) \Big/ \sum_{k=1}^{3} n_3(k)$$

and (7)

$$\xi_2 = \xi_1 \left(\sum_{k=18}^{20} n_2(k) \Big/ \sum_{k=1}^{3} n_1(k) \right),$$

where $n_i(k)$ are the counts of the kth data points in the ith data set (i=1,2,3). Furthermore, the spectrum of each detector cell was normalized to the 16th cell by equalizing the summed counts in the same energy ranges. The final spectrum in the $E_{\rm th}$ region is shown in Fig. 12.

VI. χ^2 ANALYSIS

The narrower the energy range analyzed is, the smaller the ambiguities in energy-dependent corrections are. The spectra in the $E_{\rm th}$ region and the E_0 region were therefore analyzed separately. The E_0 value extracted from the latter was used to assess the result from the former. The following analysis is different from that reported in Ref. [22] in treating the normalization constants, ξ_1 and ξ_2. However, the result is not significantly different.

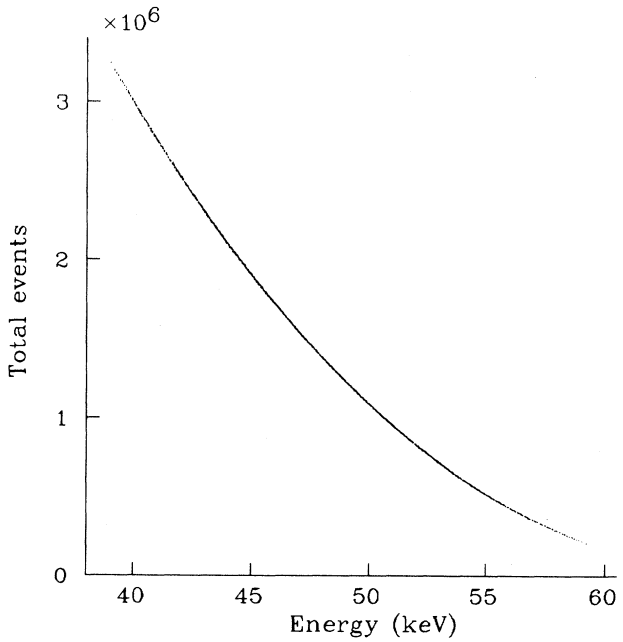

FIG. 12. ^{63}Ni spectrum measured around the 17 keV neutrino threshold ($E_{\rm th}$), consisting of 1800 data points. See the text for details.

A. Formula

The following formula was used to fit the data:

$$N^{\rm obs}(E) = A_0 \int [N^{\rm th}(E')\{1+\alpha(E_0-E')\}R(E',E)]dE' + B(E), \quad (8)$$

$$N^{\rm th}(E') = F(Z,E')p'E'_T \times \{ (1-|U|^2)(E_0-E')^2 + |U|^2 (E_0-E')\sqrt{(E_0-E')^2 - m^2_{\nu_H}} \}, \quad (9)$$

where E_T is the total energy of the β ray, A_0 is the normalization constant, and α is the shape correction factor. $|U|^2$ expresses the mixing strength of a heavy neutrino of mass m_{ν_H}. $F(Z,E)$ is the radiatively corrected, relativistic Fermi function [28]. The background spectrum is represented by $B(E)$, comprising a constant and a small linear term.

B. E_0 region

The three sets of scans made at around the end point (E_0) were combined into a single spectrum by using the normalization factors ξ_1 and ξ_2 in Eq. (7) that were evaluated from the data near $E_{\rm th}$. Ambiguities arising from this procedure are negligible compared to the statistical accuracies of the data in question.

In the energy region near E_0, the shape correction factor (α) has only a small effect. The low-energy tail of $R(E)$ also plays a minor role in the integration of Eq. (8), since the energy range to be considered here is narrow. In addition, the emission threshold ($E_{\rm th}$) of the heavy neutrino is much lower. Consequently, one can determine a reliable value for E_0 under clean circumstances. It would provide us with a very valuable means of making consistency checks on our analyses of the entire spectra.

A χ^2 fit was made to the spectrum between 63 and 74 keV with both α and $|U|^2$ set to zero. The fitting variables were A_0, E_0, and two parameters of $B(E)$. The result is shown in Fig. 13 and the best-fit value is

$$E_0 = (66\,945.9 \pm 4.4)\ {\rm eV}, \quad (10)$$

with $\chi^2/N_{\rm DF}$(number of degrees of freedom)=116.6/102. A similar fit was repeated with and without α as an additional parameter and by changing the low end of the fitted data points in 0.5 keV steps from 62.0 to 64.5 keV. The resulting values of E_0 and $B(E)$ were very stable. Therefore, the background $B(E)$ determined here was used in the following analyses. The value of α was consistent with zero with large errors.

C. Individual fits for $E_{\rm th}$ region

30 sets of spectra, each consisting of 60 data points at around $E_{\rm th}$, were individually analyzed under the assumption that m_{ν_H}=17 keV. The normalization factors

(ξ_1 and ξ_2) were not applied here. Instead, the following six parameters were treated as being free: $|U|^2$, α, three normalization constants [A_0^j (j=1,2,3)] corresponding to the three scan sets, and E_0. Other cases were also examined with E_0 being fixed to the measured value [Eq. (10)] or with $|U|^2$ set to 1%.

Figure 14 compares the best fits and the data: (a) for six parameters and (b) for five parameters with $|U|^2$=1%. For case (b), the fit clearly becomes worse near 50 keV, the expected neutrino production threshold. The qualities of the fits are shown in Fig. 15(a) as the reduced χ^2 values for the 30 spectra. Systematically larger χ^2 values are seen for the case with $|U|^2$=1%. The best-fit $|U|^2$ values are plotted in Fig. 15(c). The average over the 30 individual results gives

$$\langle |U|^2 \rangle = (-0.029 \pm 0.038)\% \quad (11)$$

with $\chi^2/N_{\rm DF}$=1.13 ($N_{\rm DF}$=29). It is consistent with zero; in fact, the average of the reduced χ^2 values is 1.01 for $|U|^2$ being free, while it jumps up to 1.45 for $|U|^2$=1%. The five-parameter fit with E_0 fixed also leads to $\langle |U|^2 \rangle$=(−0.022±0.033)% with $\chi^2/N_{\rm DF}$=1.26.

The other parameters determined in the fits are plotted in Fig. 16. When $|U|^2$ is left free, the average of 30 E_0

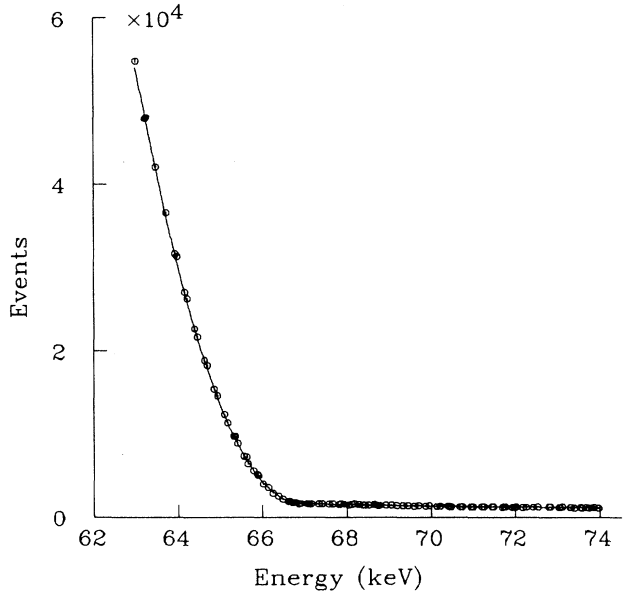

FIG. 13. ^{63}Ni spectrum measured near the end point, E_0. The curve is the best fit which gives a precise value of E_0.

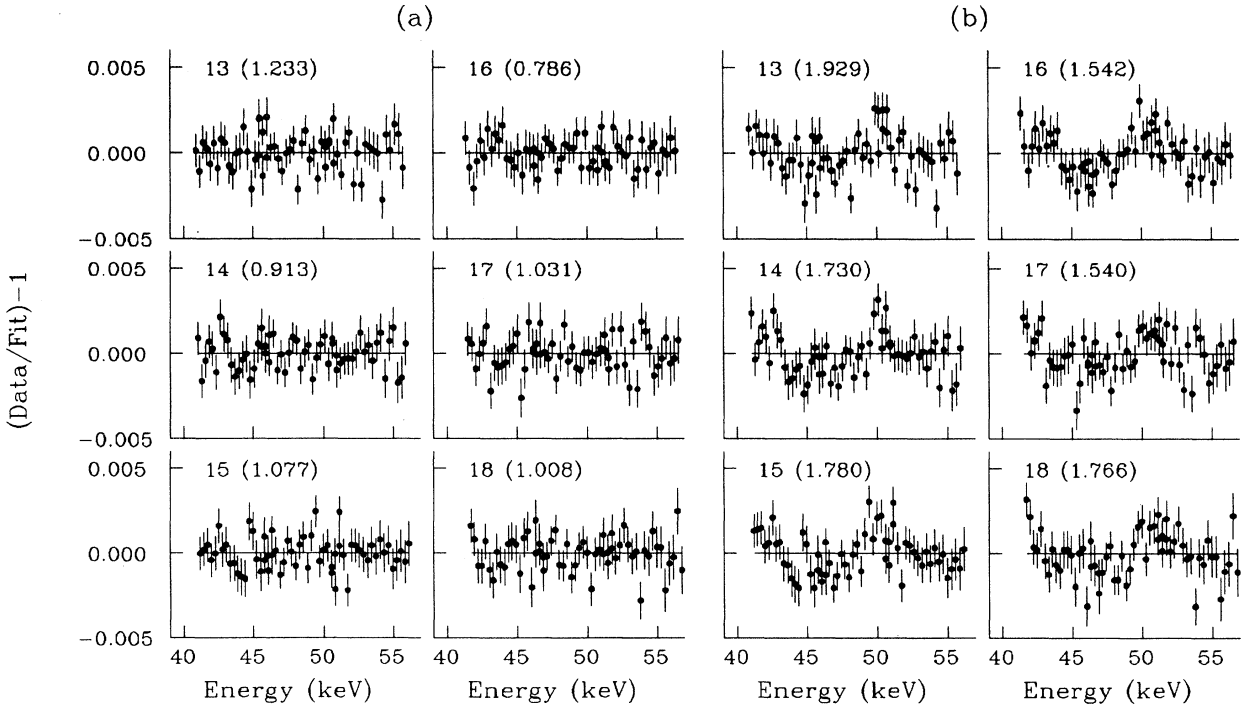

FIG. 14. Examples of the fits to individual ^{63}Ni spectra measured in the energy region around $E_{\rm th}$. Six spectra corresponding to the detector cells from the 13th to the 18th are plotted relative to the best fits. (a) and (b) show the results of the fit with $|U|^2$ left free and with $|U|^2$=1%, respectively. Shown at the top of each spectrum are the cell number and the reduced χ^2 value (in parentheses) of the fit.

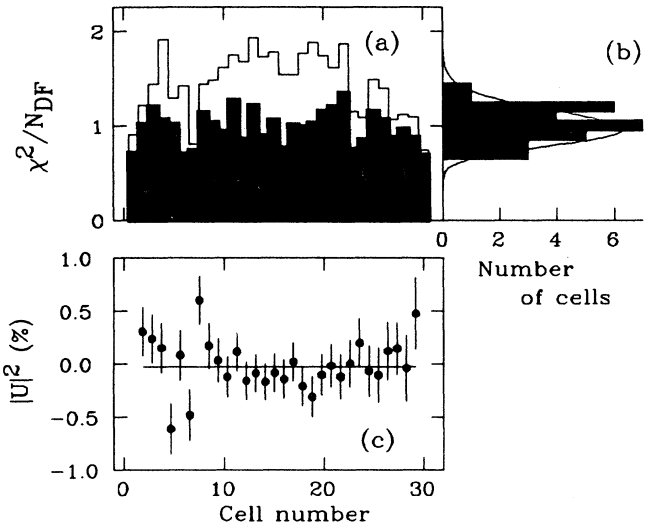

FIG. 15. Result of individual fits. (a) Reduced χ^2 values where the closed histogram comes from a fit with $|U|^2$ left free and the open histogram from the fit with $|U|^2$=1%. The distribution of the χ^2 values are plotted in (b), where the curve represents an ideal one for a Gaussian distributed random variable for N_{DF}=54. (c) The best-fit $|U|^2$ values.

values is

$$\langle E_0 \rangle = (66\,942.8 \pm 5.5)\ eV, \tag{12}$$

which agrees very well with the measured E_0=(66 945.9±4.4) eV, [Eq.(10)], as can be seen in Fig. 16(a). On the other hand, if $|U|^2$ is set to 1%, the resulting average E_0 is lower by 61.5 eV. The size of α given in Fig. 16(b) is on the order of 10^{-4} (keV)$^{-1}$ when $|U|^2$ is left free. Finally, two ratios of the normalization constants, A_0^1/A_0^3 and A_0^2/A_0^3, are compared with those independently evaluated in the previous section in terms of ξ_1 and ξ_2. Figures 16(c) and 16(d) show such a comparison. The dotted lines indicate the statistical uncertainties involved in the ξ values. The two different methods of normalization give consistent results only when $|U|^2$ is not fixed. In conclusion, the cases with $|U|^2$=1% are significantly disfavored in several aspects: χ^2, E_0, α as well as the normalization.

Figure 17 displays the variation of χ^2 with $|U|^2$ for the 30 spectra, showing that the χ^2 minima are well defined and that all of the best-fit values cluster around zero. Correlations between the variables are shown in Fig. 18 as χ^2 contour plots: α-$|U|^2$, α-E_0, and E_0-$|U|^2$.

D. Global fits for the E_{th} region

Next, a global fit was performed to all of the 1800 data points with 122 fitting parameters: α and A_0^j (j=1,2,3) for each detector cell and two common variables, E_0 and $|U|^2$. The best fit shown in Fig. 19(a) resulted in

$$|U|^2 = (-0.011 \pm 0.033)\% \tag{13}$$

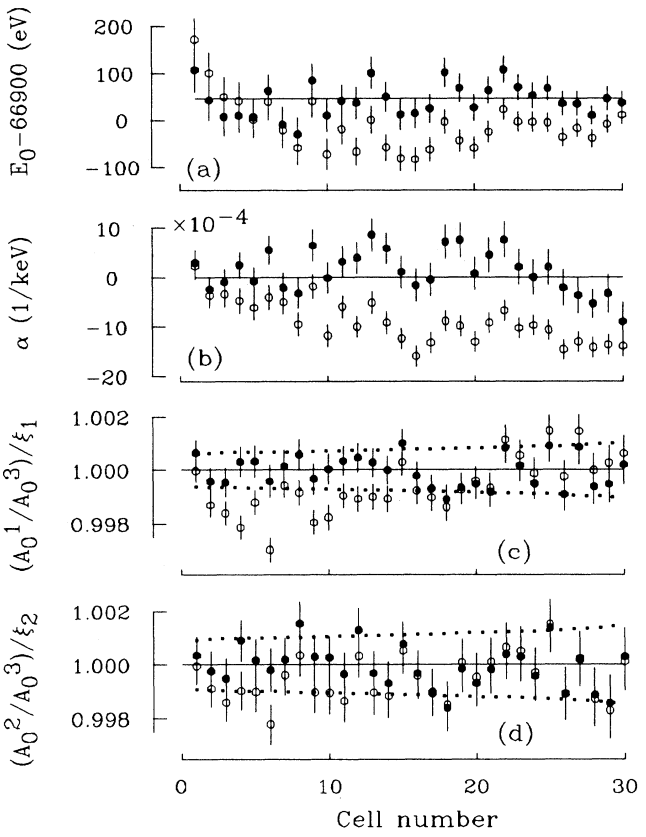

FIG. 16. Various parameters resulting from individual fits, made with $|U|^2$ left free (closed circles) and with $|U|^2$=1% (open). (a) The end point energy. The line is the one determined from the data taken near E_0 itself, Eq. (10). (b) The shape correction factor α. (c) and (d) Ratios of normalization constants for three data sets, compared with those (ξ_1 and ξ_2) obtained from the counts in the overlapped region. The dotted curves indicate the statistical uncertainties involved in ξ's.

and

$$E_0 = (66\,943.3 \pm 4.1)\ \text{eV}, \tag{14}$$

with χ^2/N_{DF}=1701.1/1678=1.01 (also see Fig. 20). All of the other parameters turned out to be similar to those obtained from the individual fits. The curve simply illustrates the size of the hypothetical 1% mixing for the 17 keV neutrino. When $|U|^2$ was fixed to 1%, the resulting E_0=66 882.3±4.6 eV was off by 63.6 eV from Eq. (10), and the fit was considerably worse, as can be seen in Fig. 19(b), giving χ^2/N_{DF}=2466.9/1679=1.47. It should be noted here that, as the figure shows, since the statistical weight of the data points was well equalized over the whole energy region, the fit was not locally biased. The result of the global fit, Eq. (13), agrees very well with Eq. (11) obtained from the individual fits.

Possible sources of systematic errors are the remaining ambiguities in the β-ray transmission through the detec-

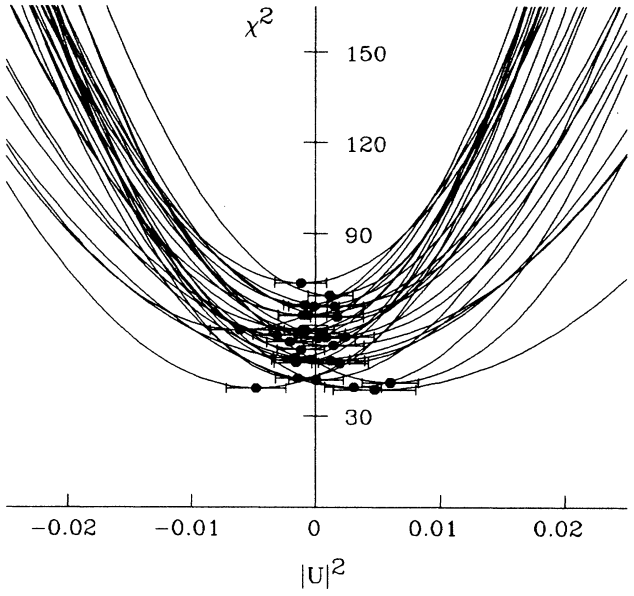

FIG. 17. χ^2 curves vs $|U|^2$ for individual spectra (N_{DF}=55 each). The closed circles are the best-fit $|U|^2$ values.

tor window, the low-energy tail of the response function [$R(E)$] and the background shape [$B(E)$]. To evaluate their effects on the final physics outputs, fits were made by varying the individual factors within the ranges estimated in Sec. V. The results are listed in Table I. The overall systematic errors were obtained by quadratically adding these uncertainties, giving ±0.03% for $|U|^2$ and ±11.5 eV for E_0. Consequently, our final result for the 17 keV neutrino is

$$|U|^2 = [-0.011 \pm 0.033(\text{stat}) \pm 0.030(\text{syst})]\% \quad (15)$$

and

$$|U|^2 < 0.073\% \quad (95\%\ \text{C.L.}). \quad (16)$$

All of the results described in this section are summarized in Table II.

E. Search for a different mass of the heavy neutrino

A global fit was also performed while searching for heavy neutrinos of different mass. Fit and error evaluations were carried out in the same manner as described above. Figure 21 shows the best-fit $|U|^2$ values as well as the 95% confidence upper limit on them. Where the fit resulted in a negative value of $|U|^2$, it was set to zero in evaluating the corresponding limit. No evidence was found for heavy neutrinos. In conclusion, the upper limit on the heavy-neutrino admixture is 0.15% (95% C.L.) in the mass range 10.5–25.0 keV.

VII. DISCUSSION

A. Normalization

The energy region around E_{th} was measured by three partly overlapped sets of scans; therefore, two normalization factors were introduced in the fits described in the previous section. In a previous publication [22], on the other hand, the normalization had not been treated as free parameters. Instead, it had been uniquely determined by calculating the ξ_1 and ξ_2 as given by Eq. (7). These different methods were systematically compared in this paper, as already shown in Fig. 16. It is concluded that the physics results do not depend on the normalization method.

B. Smoothness of the spectrum

The heavy-neutrino component near the emission threshold should exhibit an energy dependence that is quite different from the shape correction term. In fact, as already shown in Fig. 19(b), a fit with $|U|^2$=1% resulted

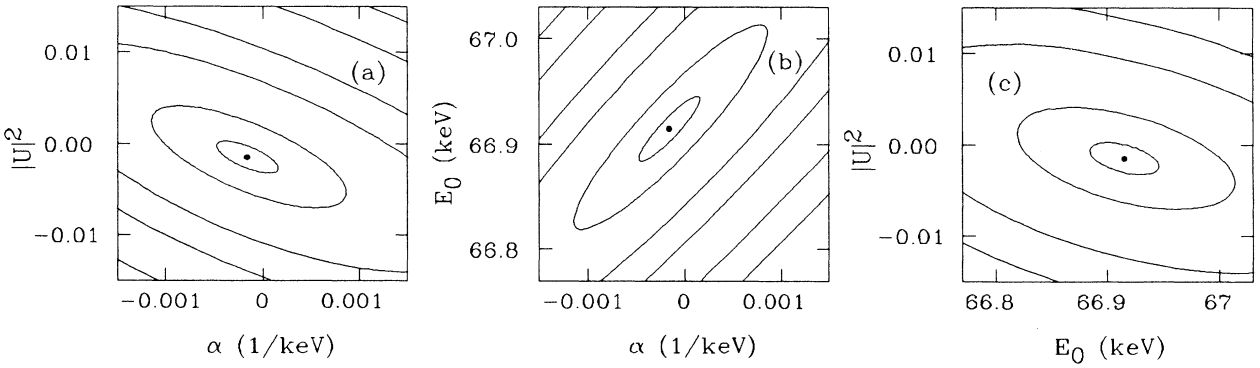

FIG. 18. χ^2 contour curves for the spectrum measured by the 16th detector cell, showing correlations between the fit parameters; (a) $|U|^2$ vs α, (b) E_0 vs α, and (c) $|U|^2$ vs E_0. The contours correspond to $\Delta\chi^2=\chi^2-\chi^2_{min}$ of 1, 10, 50, 100, 200, and 300 from inside to outside.

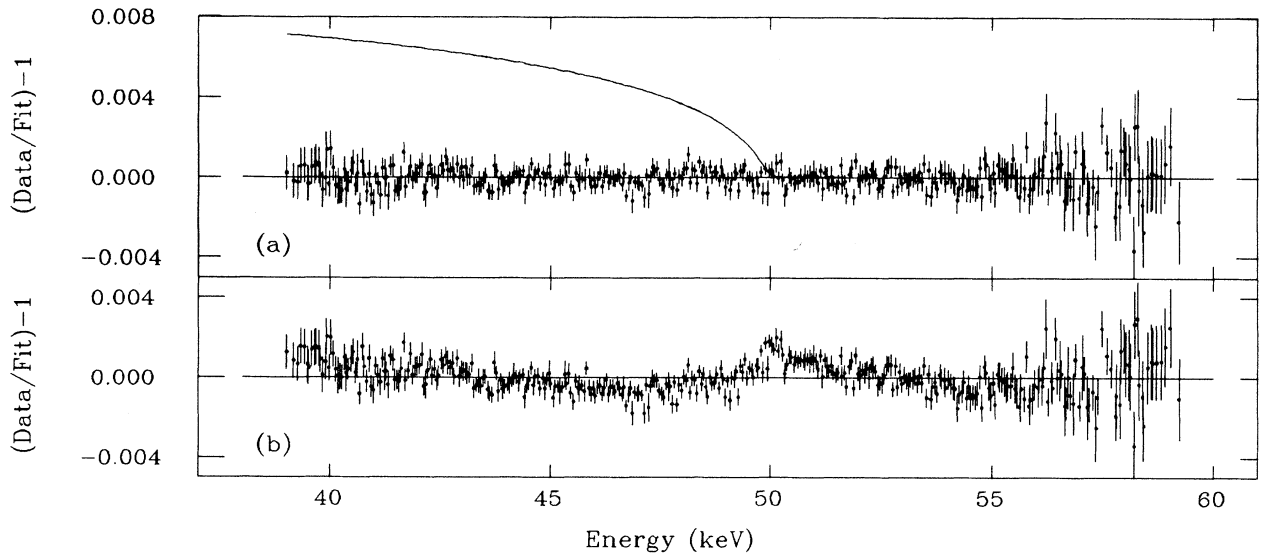

FIG. 19. The data in the $E_{\rm th}$ region plotted relative to the best global fit, (a) with $|U|^2$ free and (b) $|U|^2$=1%. For the sake of illustration, deviations of data points are binned into every 50 eV. The curve in (a) illustrates the size of a 1% mixing effect of the 17 keV neutrino.

TABLE I. Evaluation of systematic ambiguities.

Source of ambiguity	Change in parameter	Effect on $\lvert U\rvert^2$, E_0	χ^2 for $N_{\rm DF}$=1678
Window film thickness	+5%	−0.024%, +5.2 eV	1701.0
	−5%	+0.002%, −5.9 eV	1701.8
Tail in $R(E)$	Positive side (Fig. 11)	+0.018%, −8.3 eV	1702.9
	Negative side (Fig. 11)	−0.037%, +11.9 eV	1701.5
Background shape $B(E)$		Negligibly small	

TABLE II. Results of various fits with m_{ν_H}=17 keV. The number in angular brackets is the average of the 30 resultant values obtained by the individual fits. Details are described in the text.

	χ^2	$N_{\rm DF}$	$\lvert U\rvert^2$ (%)	E_0–66 900 (eV)
Fit near E_0				
	116.6	102	fixed to 0.0	45.9±4.4
			E_0=[66 945.9±4.4(stat)±3.2(sys)] eV	
Individual fits				
near $E_{\rm th}$			Fixed to 1.0	Fixed to 45.9
			⟨-0.022±0.033⟩	Fixed to 45.9
			Fixed to 1.0	⟨−18.7±4.6⟩
			⟨−0.029±0.038⟩	⟨ 42.8±5.5⟩
			$\lvert U\rvert^2$=(−0.029±0.038±0.028)%, $\lvert U\rvert^2$ < 0.077% at 95% C.L.	
			systematic errors; ±0.014% (window trans.), ±0.024% (R-tail)	
Global fits				
near $E_{\rm th}$	2744.3	1680	Fixed to 1.0	Fixed to 45.9
	1701.0	1679	−0.024±0.033	Fixed to 45.9
	2466.9	1679	Fixed to 1.0	−17.7±4.6
	1701.1	1678	−0.011±0.033	43.3±4.1
			$\lvert U\rvert^2$=(−0.011±0.033±0.030)%, $\lvert U\rvert^2$< 0.073% at 95% C.L.	
			systematic errors; ±0.013% (window trans.), ±0.027% (R-tail)	
			E_0=[66 943.3±4.1(stat)±11.9(sys)] eV	
Study of smoothness				
(see text)			⟨−0.008⟩	Fixed to 45.9

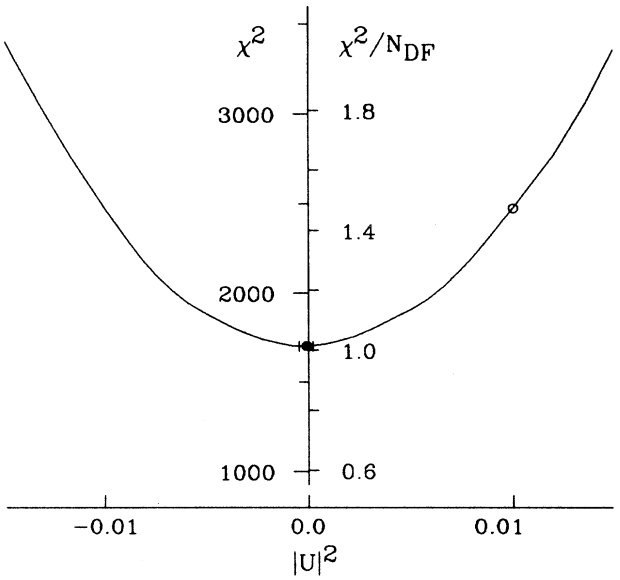

FIG. 20. χ^2 vs $|U|^2$ in the global fit to 1800 data points (N_{DF}=1678) at around E_{th}. The closed circle is the best-fit value; it changes to an open circle when $|U|^2$ is fixed to 1%.

in a sharp artificial structure at the threshold energy, even though the shape correction term and others were allowed to vary freely. Therefore, the absence of a 1% heavy-neutrino admixture can also be checked by determining whether the data constitute a single monotonous spectrum.

The data were divided into two: above and below E_{th}=50 keV. In this case, the relative normalization between different data sets was carried out based on the calculated ξ_1 and ξ_2 values. First, being free from the heavy-neutrino effect, 30 individual spectra above E_{th} were fit with two variables, α and A_0. E_0 was fixed to the value given by Eq. (10) and $|U|^2$ to zero. The thus-obtained best fit was then extrapolated to the region below E_{th}, and was then compared with the data there. The average of the resulting 30 χ^2/N_{DF} values, shown in Fig. 22(a), was 1.52; this can be compared with 21.72, which was obtained in a similar comparison made with $|U|^2$=1%.

Another check was made by fixing all of the parameters, but $|U|^2$ to those obtained above E_{th}. The $|U|^2$ value was then extracted from a fit to each of the 30 spectra below E_{th}, and is plotted in Fig. 22(b); a small error resulted from fits made without making any allowance for uncertainties in α and A_0. When averaged over 30 results, it was $\langle |U|^2 \rangle = (-0.8 \pm 0.7) \times 10^{-4}$ with $\langle \chi^2/N_{DF} \rangle = 0.97$.

In conclusion, the observed spectra are smooth across the threshold energy, and no structure is seen which can be attributed to the existence of a heavy neutrino. The $|U|^2$ value obtained in the present fits is consistent with zero, in very good agreement with the conclusion of the previous section.

C. End-point energy

The result of an absolute energy calibration is, in good part, affected by the reproducibility in the source position as well as the stability of the magnetic field. Its

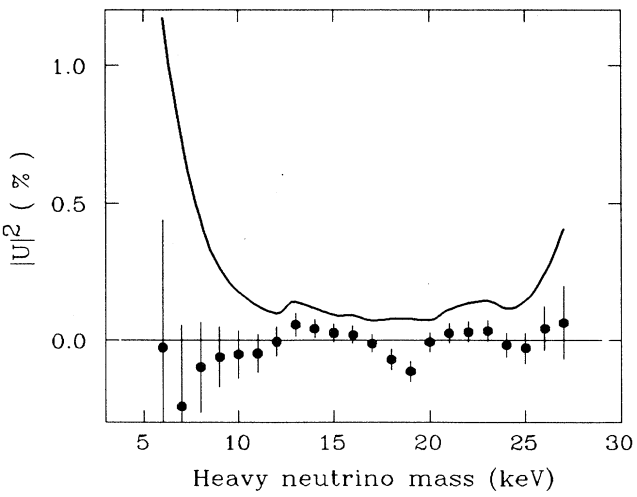

FIG. 21. Best-fit $|U|^2$ values as a function of the hypothetical heavy neutrino mass. The closed circles are the result with statistical errors. The upper limit at the 95% C.L. is evaluated with systematic errors and is shown by the curve.

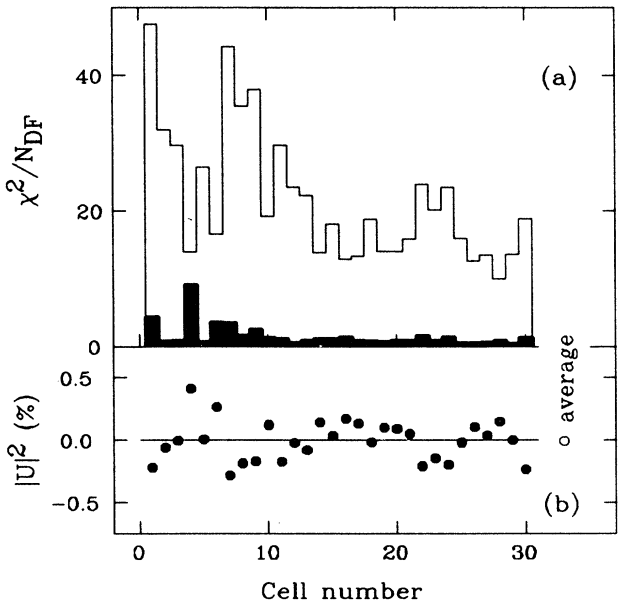

FIG. 22. Result of testing the smooth continuation of the Ni spectrum across E_{th}. (a) Comparison of data for E <50 keV with an extrapolation of the best fit obtained with data for E >50 keV. The reduced χ^2 values are plotted for 30 spectra; the closed histogram results from the case with $|U|^2$=0% and the open histogram with $|U|^2$=1%. (b) $|U|^2$ values resulting from a single-parameter fit to the data for E <50 keV, where the other parameters were given from an independent fit made to the data above 50 keV.

uncertainty was evaluated to be ±3.2 eV at the end point (E_0). The other contribution from uncertainties in the transmission through the detector window, and the response function [$R(E)$] was less than ±0.1 eV for data at around E_0 itself, and ±11.5 eV for the data taken around $E_{\rm th}$. Accordingly, the final E_0 values are given by

$$E_0 = (66\,945.9 \pm 4.4 \pm 3.2)\ \text{eV}$$

from the data around E_0 (17)

and

$$E_0 = (66\,943.3 \pm 4.1 \pm 11.9)\ \text{eV}$$

from the data around $E_{\rm th}$. (18)

Here, the first and the second errors are statistical and systematic, respectively. These two independent measurements agree very well with each other and also with E_0=(66.946±0.020) keV measured by Hetherington *et al.* [10]. This fact supports our analyses in the energy region near $E_{\rm th}$, where good knowledge concerning $R(E)$ is essential.

VIII. CONCLUSION

The present experiment directly searched for a kink in the ^{63}Ni β-ray spectrum, possibly caused by the hypothesized 17 keV neutrino emission. A high-statistics measurement was performed in fine energy steps around the expected threshold energy, thus eliminating any possibility of confusing the shape correction term with the heavy-neutrino component. No analysis found any structure in the spectrum, and the smooth monotonous spectrum was only explained as being due to a null admixture of the heavy neutrino. The resulting mixing parameter $|U|^2$ is consistent with zero:

$$|U|^2 = [-0.011 \pm 0.033(\text{stat}) \pm 0.030(\text{sys})]\%, \quad (19)$$

which is 22σ away from $|U|^2$=1%. The corresponding upper limit for the 17 keV neutrino is

$$|U|^2 < 0.073\%(95\%\ \text{C.L.}). \quad (20)$$

The present result is plotted in Fig. 1 in comparison with others.

From the same data, a search was also made for a heavy neutrino with different masses and no positive indication was found. This study sets an upper limit of

$$|U|^2 < 0.15\%(95\%\ \text{C.L.})\ \text{for}\ m_{\nu_H} = 10.5 - 25.0\ \text{keV}. \quad (21)$$

Finally, the end-point energy of ^{63}Ni β rays was determined from the two different sets of data with high accuracies. The two measurements found the following very good agreement:

$$E_0 = [66\,945.9 \pm 4.4(\text{stat}) \pm 3.2(\text{sys})]\ \text{eV}$$

from the data around E_0, (22)

$$E_0 = [66\,943.3 \pm 4.1(\text{stat}) \pm 11.9(\text{sys})]\ \text{eV}$$

from the data around $E_{\rm th}$. (23)

ACKNOWLEDGMENTS

We wish to thank Professor S. Schnetzer (Rutgers) for his significant contribution during the early stage of the experiment, and T. Yahata for his continuous cooperation. We gratefully acknowledge Professor R. G. H. Robertson (LANL) for his useful suggestions concerning the normalization factors. We thank Professors H. Sugawara (KEK), T. Yamazaki (INS), and I. Katayama (INS) for their encouragement and support, and Dr. H. Ozaki (KEK) for his helpful suggestions pertaining to the measurement. We also would like to thank Professor S. Iwata (KEK) for reading and editing this manuscript.

[1] J. J. Simpson, Phys. Rev. Lett. **54**, 1891 (1985).
[2] For instance, see M. J. Dugan *et al.*, Phys. Rev. Lett. **54**, 2302 (1985); S. L. Glashow, Phys. Lett. B **256**, 255 (1991); E. W. Kolb and M. S. Turner, Phys. Rev. Lett. **67**, 5 (1991); K. S. Babu and R. N. Mohapatra, *ibid.* **67**, 1498 (1991); C. H. Albright, Phys. Rev. D **45**, 1624 (1992); J. M. Cline and T. P. Walker, Phys. Rev. Lett. **68**, 270 (1992).
[3] A. M. Apalikov *et al.*, Pis'ma Zh. Eksp. Teor. Fiz. **42**, 233 (1985) [JETP Lett. **42**, 289 (1985)].
[4] J. Markey and F. Boehm, Phys. Rev. C **32**, 2215 (1985).
[5] T. Altzitzoglou *et al.*, Phys. Rev. Lett. **55**, 799 (1985).
[6] T. Ohi *et al.*, Phys. Lett. **160B**, 322 (1985); in *Neutrino '86: Neutrino Physics and Astrophysics*, Proceedings of 12th International Conference on Neutrino Physics and Astrophysics, Sendai, Japan, 1986, edited by T. Kitagaki and H. Yuta (World Scientific, Singapore, 1986), p. 69.
[7] V. M. Datar *et al.*, Nature **318**, 547 (1985).
[8] D. Wark and F. Boehm, in *Nuclear Beta Decays and Neutrinos*, Proceedings of the International Symposium, Osaka, Japan, 1986, edited by T. Kotani, H. Ejiri, and E. Takasugi (World Scientific, Singapore, 1986), p. 391.
[9] M. J. G. Borge *et al.*, Phys. Scr. **34**, 591 (1986).
[10] D. W. Hetherington *et al.*, Phys. Rev. C **36**, 1504 (1987).
[11] I. Žlimen *et al.*, Phys. Scr. **38**, 539 (1988).
[12] H. W. Becker *et al.*, Caltech Report No. 63-605, 1991 (unpublished); M. Chen *et al.*, Phys. Rev. Lett. **69**, 3551 (1992).
[13] A. Hime and J. J. Simpson, Phys. Rev. D **39**, 1837 (1989).
[14] J. J. Simpson and A. Hime, Phys. Rev. D **39**, 1825 (1989).

[15] A. Hime and N. A. Jelly, Phys. Lett. B **257**, 441 (1991).
[16] I. Žlimen *et al.*, Phys. Rev. Lett. **67**, 560 (1991).
[17] B. Sur *et al.*, Phys. Rev. Lett. **66**, 2444 (1991).
[18] D. R. O. Morrison (private communication): DiGregorio *et al.* found a best fit of 13.8 keV with 0.8% mixing but excluded a 17 keV neutrino.
[19] C. D. Ellis and W. J. Henderson, Proc. R. Soc. London **A146**, 206 (1934).
[20] E. J. Konopinski and G. E. Uhlenbeck, Phys. Rev. **48**, 7 (1935).
[21] For instance, see C. S. Wu and R. D. Albert, Phys. Rev. **75**, 315 (1948); C. S. Cook, L. M. Langer, and H. C. Price, Jr., *ibid.* **74**, 547 (1948); L. M. Langer and R. J. D. Moffat, *ibid.* **88**, 548 (1952). A review at that time on nuclear β decay can be found in E. J. Konopinski, Rev. Mod. Phys. **15**, 209 (1943).
[22] H. Kawakami *et al.*, Phys. Lett. B **287**, 45 (1992). Because of the author's typographical error, the statistical error of E_0, ± 2.7 eV in Eq. (2) of this reference should be replaced by ± 4.4 eV.
[23] H. Kawakami *et al.*, Phys. Lett. B **256**, 105 (1991); J. Phys. Soc. Jpn. **57**, 2873 (1988); Phys. Lett. B **187**, 198 (1987).
[24] T. Tabata, R. Ito, and S. Okabe, Nucl. Instrum. Methods **103**, 85 (1972).
[25] M. Fujioka and K. Kageyama, in *Proceedings of 1981 INS International Symposium on Nuclear Radiation Detectors*, Tokyo, Japan, 1981, edited by K. Husimi and Y. Shida (Institute for Nuclear Physics, Tokyo, 1981), p. 589.
[26] J. A. Bearden and A. F. Burr, in *CRC Handbook of Chemistry and Physics*, 70th ed., edited by R. C. Weast, D. R. Lide, M. J. Astle, and W. H. Beyer (CRC Press, Boca Raton, Florida, 1990), p. E-191.
[27] H. Kawakami *et al.*, Phys. Lett. A **121**, 414 (1987).
[28] A. Sirlin, Phys. Rev. **164**, 1767 (1967); D. H. Wilkinson and B. E. F. Macefield, Nucl. Phys. **A158**, 110 (1970).